

## **Constraints on velocity-depth trends from rock physics models**

Peter Japsen<sup>1</sup>, Tapan Mukerji<sup>2</sup> and Gary Mavko<sup>2</sup>

<sup>1</sup> Geological Survey of Denmark and Greenland (GEUS), Øster Voldgade 10, DK-1350 Copenhagen, Denmark. pj@geus.dk,

<sup>2</sup> Stanford Rock Physics Laboratory, Stanford University, California 94305, USA.

### **ABSTRACT**

Estimates of depth, overpressure and amount of exhumation based on sonic data for a sedimentary formation rely on identification of a normal velocity-depth trend for the formation. Such trends describe how sonic velocity increases with depth in relatively homogenous, brine-saturated, sedimentary formations as porosity is reduced during normal compaction (mechanical and chemical). Compaction is ‘normal’ when the fluid pressure is hydrostatic, and the thickness of the overburden has not been reduced by exhumation. We suggest that normal porosity at the surface for a given lithology should be constrained by its critical porosity, the porosity limit above which a particular sediment exists only as a suspension. Consequently, normal velocity at the surface of unconsolidated sediments saturated with brine approaches the velocity of the sediment in suspension. Furthermore, porosity must approach zero at infinite depth, so the velocity approaches the matrix velocity of the rock, and the velocity-depth gradient approaches zero. For sediments with initially good grain contact (when porosity is just below the critical porosity) the velocity gradient decreases with depth. In contrast, initially compliant sediments may have a maximum velocity gradient at some depth if we assume porosity to decrease exponentially with depth. We have used published velocity-porosity-depth relationships to formulate normal velocity-depth trends for

consolidated sandstone with varying clay content and for marine shale dominated by smectite/illite. The first is based on a modified Voigt trend (porosity scaled by critical porosity), and the second is based on a modified time-average equation. Baselines for sandstone and shale in the North Sea agree with the established constraints and the shale trend can be applied to predict overpressure. A normal velocity-depth trend for a formation can not be expressed from an arbitrary choice of mathematical functions and regression parameters, but should be considered as a physical model linked to the velocity-porosity transforms developed in rock physics.

## **INTRODUCTION**

A normal velocity-depth trend is a function describing how sonic velocity increases with depth in a relatively homogenous, brine-saturated sedimentary formation when porosity is reduced during normal compaction (mechanical or chemical). Compaction is ‘normal’ when the fluid pressure of the formation is hydrostatic, and the formation is at maximum burial depth; i.e., the thickness of the overburden has not been reduced by exhumation. The term baseline is frequently used as a synonym for a normal velocity-depth trend, typically to refer to reference trends established from a given database. The sonic velocity may be represented by the velocity,  $V$  [m/s].

Velocity-depth studies are useful because they are based on easily accessible data with a wide lateral and vertical coverage, and can thus prescribe simple constraints on both physical and geological parameters because acoustic waves are affected by bulk properties as they propagate through the sediment. Disagreement between predicted and measured velocity,  $V$  [m/s], at a given depth may indicate that a formation has become overpressured due to rapid burial (resulting in lower velocity than expected) or that the overburden has been partially removed subsequent to maximum burial (resulting in

higher velocity than expected) (Figure 1). A velocity-depth anomaly can also be measured along the depth axis as the burial anomaly,  $dZ_B$  [m] (Japsen 1998). Velocity-depth trends are used for:

- Estimating amount of removed overburden ('uplift') relative to an overcompacted formation (e.g., Acheson 1963; Magara 1978; Bulat and Stoker 1987; Japsen 1993; 1998; 2000; Hillis 1995; Hansen 1996b; Heasler and Kharitonova 1996; Ware and Turner 2002; Corcoran and Doré 2005; Corcoran and Mecklenburgh 2005).
- Estimating overpressure due to undercompaction (e.g., Hottmann and Johnson 1965; Magara 1978; Chapman 1983; Japsen 1998; 1999; Winthaege and Verweij 2003).
- Converting traveltimes to depth (e.g., Slotnick 1936; Japsen 1993; Al-Chalabi 1997b).
- Determining background velocity – or the low frequency model – for inversion of seismic data (e.g. Snieder et al. 1989).
- Modeling the manner in which amplitude variation with offset (AVO) intercept and gradient change with increasing burial (e.g. Smith and Sondergeld 2001).

Rock physics relations, such as the Wyllie et al. (1956) empirical time-average, the Raymer et al. (1980) relations, or the modified Voigt model (Nur et al. 1998), relate velocity to porosity for different rock types (cf. Dvorkin et al. 2002). But even though the concept of velocity-depth trends is as old as exploration geophysics (e.g., Slotnick 1936; Haskell 1941), few attempts have been made to constrain them for different lithologies rather than just considering velocity-depth trends as fits of arbitrary functions to local data sets.

Chapman (1983) combined the time-average equation with exponential decay of porosity with depth and thus derived an expression for the increase of shale velocity with depth that is constrained by the velocity of the sediment at the surface and does not approach infinite velocity at depth. Bulat and Stoker (1987) and Hillis (1995) estimated baselines for different lithologies but did not consider that rock physical properties influence the curvature of velocity-depth trends and that velocity is finite even at great depth. Japsen (1998; 1999; 2000) defined normal velocity-depth trends for chalk and shale in a way that the predicted velocities agreed with those of recent deposits at the surface and that they did not approach infinity at depth. Velocity-depth anomalies relative to these trends were found to be in agreement with estimates of amount of exhumation along the margins of the North Sea Basin as well as with measurements of overpressure in the centre of this basin.

Much empirical and theoretical insight into the physics of rocks has been gained since the formulation of the time-average equation, and consequently the analysis of Bulat and Stoker (1987) and others can be refined. In this paper we investigate how joining rock physics  $V$ - $\phi$  models with the  $\phi$ - $z$  relationship during normal compaction for the rock in question can introduce sensible, simple constraints on  $V$ - $z$  trends ( $z$  is depth below sea bed or ground level [m], and  $\phi$  is porosity [fraction]). We find that the normal velocity at the surface for a given rock is constrained by its critical porosity, and demonstrate that differences in the initial grain contact in sandstone and shale influence the curvature of the velocity-depth trends for these sediments ( $k$  is the velocity-depth gradient [ $\text{m/s/m}=\text{s}^{-1}$ ]). We conclude that normal velocity-depth trends should be considered as physical models for specific lithologies.

## **ROCK PHYSICS MODELS**

### **Critical porosity**

For most porous materials, there appears to be a critical porosity,  $\phi_c$ , that separates mechanical and acoustic behaviour into two distinct domains (Nur et al. 1991; Chen and Nur 1994; Nur et al. 1998). By definition  $\phi_c$  is the porosity below which the mineral grains in a sediment become load-bearing. At porosities above  $\phi_c$ , the sediment loses all rigidity and falls apart: the sediment is in suspension and the fluid phase is load-bearing. Critical porosity has also been called elastic percolation porosity (Feng and Sen 1985; Guéguen et al. 1997) or the pre-compaction porosity (Nolen-Hoeksema 1993).

The transition from suspension to solid is implicit in the empirical velocity-porosity relation of Raymer et al. (1980). If critical porosity is exceeded at the time of initial deposition of grains, they are barely in contact, and consequently have no rigidity (Guéguen and Palciauskas 1994). The value of  $\phi_c$  is determined by sediment type, grain sorting and angularity at deposition, and can thus vary within the same rock type (Table 1a). The concept of critical porosity is developed for sediments saturated with brine, and the arguments presented here do not necessarily apply for e.g. aeolian sediments. Critical porosity behaviour is a general geometric property, and is a powerful constraint on theoretical models.

### **V- $\phi$ trajectories**

The velocity (or effective modulus) of a rock with a given porosity and fluid composition always falls between the Voigt upper and the Reuss lower bounds, but its precise value depends on the geometric details of the grain-pore microstructure (see Appendix A). Stiffer pore shapes cause the velocity to be closer to the upper bound;

softer or more compliant shapes cause the velocity to be lower (e.g. Mavko et al. 1998). When compaction and diagenesis reduce porosity and thus increase the elastic stiffness, data points for a given rock type and diagenetic history will thus fall along a specific path or trajectory ( $V$ - $\phi$  path) in a plot of velocity versus porosity:

**Initially stiff rocks:** The  $V$ - $\phi$  path is concave for rocks that show a strong increase in velocity for porosity reduction just below the critical porosity (curve  $V_N^{ss10}$  in Figure 2, e.g. consolidated sandstone):

$$\left(\frac{dV}{d\phi}\right)_{\phi \approx \phi_c} \ll 0, \quad \frac{d^2V}{d\phi^2} < 0$$

A concave  $V$ - $\phi$  curve has a negative second derivative. The initial sensitivity to porosity reduction may be due to the growth and cementation of grain contacts (e.g., Dvorkin and Nur 1996), while mechanical compaction is limited. In this paper we refer to such rocks as “initially stiff rocks”.

**Initially compliant rocks:** The  $V$ - $\phi$  path is convex for rocks that show a weak increase in velocity for porosity reduction just below the critical porosity close to  $\phi_c$  (curve  $V_N^{sh}$  in Figure 2, e.g., shale, chalk):

$$\left(\frac{dV}{d\phi}\right)_{\phi \approx \phi_c} \approx 0, \quad \frac{d^2V}{d\phi^2} > 0$$

A convex  $V$ - $\phi$  curve has a positive second derivative. This initial insensitivity to porosity reduction may be attributed to dominance of compaction, poor sorting, and growth of pore-filling cement. In this paper we refer to such rocks as “initially compliant rocks”.

## COMPACTION TRENDS

Burial of sediment leads to initial compaction and reduction of porosity to less than  $\phi_c$ .

We therefore assume that critical porosity of the sediment is reached only at the surface when pressure remains hydrostatic. We make the important assumption that  $\phi_0$ , the porosity at the surface of the sedimentary succession, is constrained by the critical porosity of the freshly deposited sediment:

$$\phi_0 \leq \phi_c. \quad (1)$$

The geologic interpretation of this statement is that, at least for clastics, the weak suspension state at critical porosity describes the sediment when it is first deposited, before compaction and diagenesis. The overall agreement between independent estimates of  $\phi_c$  and  $\phi_0$  for different rock types support the assumption that the limiting porosity at the surface is close to the critical porosity; e.g., for chalk  $\phi_0=70\%$  (Scholle 1977) and  $\phi_c=65\%$  (Nur et al. 1998; cf. Fabricius 2003) (see Table 1a).

The porosity-reduction in sedimentary rocks during normal compaction has frequently been approximated by exponential functions (e.g., Athy 1930; Rubey and Hubbert 1959; Magara 1978; Sclater and Christie 1980; Hansen 1996a). Exponential functions have convenient mathematical properties, and predict a physically constrained variation of porosity. Exponential porosity decay is a first order approximation and thus does not include e.g. onset of cementation below a certain depth. If we apply this approximation and set porosity at the surface to  $\phi_c$ :

$$\phi = \phi_c e^{-z/\beta} = \phi_c e^{-z/\beta}, \quad (2)$$

where the constant  $\beta$  [m] is a measure of the rate of porosity decay. The assumption of  $\phi_0=\phi_c$  allows us to link knowledge from rock physics with compaction trends.

## NORMAL VELOCITY-DEPTH TRENDS

### General conditions

We will consider velocity as a function of porosity and porosity as a function of depth:

$$V(z) = V[\phi(z)]$$

where  $z$  may range from the surface to infinite depth. The velocity-depth gradient,  $k$  [m/s/m = s<sup>-1</sup>], can be calculated by differentiation of the above expression:

$$k = \frac{dV}{dz} = \frac{d}{dz}V[\phi(z)] = \frac{d}{d\phi}V(\phi) \cdot \frac{d}{dz}\phi(z), \quad (3)$$

meaning that the shape of the  $V$ - $z$  trend depends on the shape of the  $V$ - $\phi$  and the  $\phi$ - $z$  curves. As both terms on the right are negative or zero, we get  $k \geq 0$  (cf. Figure 2c).

We can set up three simple boundary conditions for  $V(z)$  for  $z = 0$  and  $z \rightarrow \infty$ :

- $V_0 \geq V_c$ . The velocity of unconsolidated sediments at the surface,  $V_0$ , is constrained by the velocity at critical porosity,  $V_c$  given by the Reuss average at  $\phi_c$  (equation A-1). This follows from equation (1).  $V_0$  will thus in general differ from the velocity of water (Tables 1b, c).
- $V_\infty \rightarrow V_m$ . Since porosity at infinite depth approaches zero, the velocity,  $V_\infty$  of the sedimentary rock at infinite depth approaches the velocity at zero porosity, the velocity,  $V_m$ , of the matrix mineral at high pressure and temperature.
- $k \rightarrow 0$  for  $z \rightarrow \infty$ . The velocity-depth gradient must approach zero at infinite depth as velocity can not increase beyond the finite value of  $V_m$ .

### Assuming exponential form for $\phi$ - $z$ trends

We can simplify the relation between velocity and depth by introducing exponential po-

rosity decay with depth (equation 2):

$$V(z) = V[\phi(z)] = V(\phi_0 e^{-z/\beta}).$$

The velocity-depth gradient is found by making the same substitution into equation (3):

$$k = \frac{dV}{d\phi} \cdot \frac{d\phi_0 e^{-z/\beta}}{dz} = \frac{dV}{d\phi} \cdot \left(-\frac{1}{\beta} \phi_0 \cdot e^{-z/\beta}\right) = -\frac{dV}{d\phi} \cdot \phi/\beta.$$

The proportionality between  $k$  and  $dV/d\phi$  means that the shape of the  $V$ - $z$  path reflects the shape of the  $V$ - $\phi$  path. We can compare  $V$ - $z$  trends for rocks with different curvature in the  $V$ - $\phi$  plane by differentiating the above expression for  $k$  assuming exponential porosity-decay with depth (equation 2):

$$\frac{dk}{dz} = \frac{d}{dz} \left[ -\frac{dV}{d\phi} \cdot \frac{\phi}{\beta} \right] = \frac{dV}{d\phi} \cdot \frac{d}{dz} \left[ -\frac{\phi}{\beta} \right] - \frac{\phi}{\beta} \cdot \frac{d}{dz} \left[ \frac{dV}{d\phi} \right] = \frac{1}{\beta^2} \left( \frac{dV}{d\phi} + \phi \frac{d^2V}{d\phi^2} \right) \phi.$$

The first term on the right is negative for any rock, while the sign of the second term depends on the curvature of the  $V$ - $\phi$  path; i.e., positive or negative for rocks that are initially compliant or stiff, respectively (curves  $V_N^{sh}$  and  $V_N^{ss10}$  in Figure 2e):

- For initially stiff rocks ( $d^2V/d\phi^2 < 0$ ), we get  $dk/dz < 0$ , indicating that  $k(z)$  decreases monotonously with increasing depth from the surface; i.e. with no local maxima for the velocity-depth gradient (curve  $V_N^{ss10}$  in Figures 2d, f). This decreasing velocity-depth gradient at shallow depths reflects the slowdown of the velocity increase, perhaps after the initial growth and cementation of grain contacts (see the sandstone case below; Figure 3).
- For initially compliant rocks ( $d^2V/d\phi^2 > 0$ ),  $dk/dz$  may become zero (curve  $V_N^{sh}$  in Figures 2d, f). Therefore, an increasing velocity-depth gradient at shallow depths may reflect the accelerated increase of velocity as mechanical compaction takes

place, whereas the slow-down of porosity-reduction at depth leads to a decreasing velocity-depth gradient. Initially compliant rocks may thus have a maximum velocity gradient at intermediate depth due to the combined effect of these two processes (see the shale case below; Figure 4).

We investigate velocity-depth relations for specific velocity-porosity trends in Appendix B and discuss analytical functions that have been applied to represent the increase of velocity with depth in Appendix C (see also Table 2).

## **BASELINES FOR SANDSTONE AND SHALE ESTIMATED FROM NORTH SEA DATA**

It can be difficult to estimate the normal velocity-depth trend for a formation because the formation may not easily be found under normally compacted conditions; e.g. the formation may either be undercompacted due to overpressuring or it may be overcompacted due to exhumation of its overburden (Figure 1). It may however be possible to estimate the maximum burial of the formation independently: Along the margins of the North Sea Basin the amount of Cenozoic exhumation can be calculated from the burial anomaly of the thick and uniform Upper Cretaceous–Danian chalk relative to the normal velocity-depth trend for the chalk (Japsen 1998; 2000). Baselines can be more easily traced in plots of velocity versus pre-exhumation depths because the formations underlying the chalk were at maximum burial at more locations prior to the exhumation (Figure 5). Data points at shallow depth relative to the baseline may thus represent locations where the formation experienced maximum during the Mesozoic (cf. Japsen 2000).

Normal velocity-depth trends for sandstone and shale were established by

Japsen (2000) from a regional data base of interval velocities estimated in UK and Danish wells in the North Sea Basin (cf. Hillis 1995). The wells have interval velocities from a marine, Jurassic shale (the F-1 Member of the Lower Jurassic Fjerritslev Formation), from the Triassic redbeds of the Bunter Sandstone or the Bunter Shale, as well as from the North Sea Chalk. The Triassic redbeds were deposited in a supratidal or continental environment during a hot, semi-arid climate (Bertelsen 1980; Johnson et al. 1994). The Fjerritslev Formation was deposited in a marine environment (Michelsen 1989), and its clay mineralogy is dominated by smectite/illite in distal parts of the basin (H. Lindgreen, pers. comm. 2000).

### *A baseline for sandstone based on data for Triassic formations*

#### *Bunter Shale*

The plot of velocity versus pre-exhumation depths for the Bunter Shale in Figure 6b shows a reasonably well-defined trend of data points at *maximum burial* ( $2.6 < V < 4.8$  km/s). By contrast, the plot of velocity versus *present depth* in Figure 6a reveals no clear trend. Some data points plot above the trend in Figure 6b and thus represent areas where the Bunter Shale was at maximum burial prior to Cenozoic exhumation or areas of anomalous lithology.

The trend of data points at maximum burial reveals a slight curvature that reflects the decrease of the velocity gradient with depth, and this trend is approximated by 3 linear segments plus a fourth segment that connects the observed trend with a physically reasonable velocity at the surface. The normal velocity-depth trend for the Bunter Shale,  $V_N^B$  can be approximated by the following expression (Japsen, 2000):

$$\begin{aligned}
V_N^B &= 1550 + z \cdot 0.6, & 0 < z < 1393 \text{ m} \\
V_N^B &= -400 + z \cdot 2, & 1393 < z < 2000 \text{ m} \\
V_N^B &= 2600 + z \cdot 0.5, & 2000 < z < 3500 \text{ m} \\
V_N^B &= 3475 + z \cdot 0.25, & 3500 < z < 5300 \text{ m}
\end{aligned} \tag{4}$$

The gradient is  $2 \text{ s}^{-1}$  for depths around 2 km, from where it decreases gradually with depth to 0.5 and then  $0.25 \text{ s}^{-1}$ . The gradient is taken to be  $0.6 \text{ s}^{-1}$  in the upper part to arrive at a physically reasonable velocity at the surface.

### ***Bunter Sandstone***

The plot of velocity versus pre-exhumation depths for the Bunter Sandstone in Figure 7b has a trend of data at maximum burial that coincides with the trend for the Bunter Shale ( $3.0 < V < 4.3 \text{ km/s}$ ), and equation (4) is thus considered as an approximation for the observed Bunter Sandstone trend. See the section ‘ $V$ - $\phi$ - $z$  relations for consolidated sandstone’ for further discussion.

### ***A shale trend based on data for a Jurassic formation***

The plot of velocity versus pre-exhumation depths for the marine, Lower Jurassic shale in Figure 8b shows a well-defined trend of data points at maximum burial ( $2.6 < V < 3.6 \text{ km/s}$ ). A number of data points plot above the trend, and presumably represent either areas where the shale was at maximum burial prior to Cenozoic exhumation or areas of anomalous lithology. The normal velocity-depth trend for the marine shale,  $V_N^{sh}$ , can be approximated by a constrained, exponential transit time-depth model of the form given by equation (C-5) (Japsen 2000):

$$V_N^{sh} = 10^6 / (460 \cdot e^{-z/2175} + 185) \tag{5}$$

where transit time,  $tt = 1/V \cdot 10^6$  [ $\mu\text{s/m}$ ]. The trend fulfils reasonable boundary conditions at the surface and at infinite depth,  $V_0 = 1550 \text{ m/s}$  and  $V_\infty = 5405 \text{ m/s}$ , and it is

well defined at depth where velocity-depth data for normally compacted shale can be difficult to identify ( $2 < z < 4$  km). The trend has a maximum velocity-depth gradient of  $0.6 \text{ s}^{-1}$  at  $z=2.0$  km. See the section ‘ $V$ - $\phi$ - $z$  relations for shale’ for further discussion.

The depth shift between the observed trends for the Bunter and for the marine shale exceeds 1 km for  $V > 3$  km/s. This shift must be related to physical differences between the two lithologies that have the word ‘shale’ in common because an explanation related to a previous greater burial for the data points defining the Bunter trend than for the marine shale trend is not compatible with the geology of the area (see Japsen 2000).

## **CONSTRAINTS ON VELOCITY-DEPTH RELATIONS FOR SANDSTONE AND SHALE**

Here we will study the effect of porosity reduction on velocity in both the  $V$ - $\phi$  and the  $V$ - $z$  plane for rock types with depth-dependent compaction such as consolidated sandstone and shale. By estimating  $V$ - $\phi$  and  $\phi$ - $z$  relations for these lithologies we can eliminate the dependency on  $\phi$  to find likely  $V$ - $z$  trends that we can compare to the North Sea baselines that we described in the preceding section. S-wave velocity may be predicted from  $V$  (P-wave velocity) based on empirical relations for sandstone or shale (e.g. Han et al. 1986; Greenberg and Castagna 1992).

### **$V$ - $\phi$ - $z$ relations for consolidated sandstone**

#### ***$V$ - $\phi$ model***

We construct modified Voigt upper bounds to describe the  $V$ - $\phi$  trend for consolidated sandstone with varying clay content during normal compaction (Han et al. 1986; Nur et al. 1991). The velocity varies between two end-members (equation A-2): the maximum-

porosity end-member for the mineral suspension at critical porosity ( $\phi_c$ ,  $V_c$ ) (equation A-1), and the minimum-porosity end-member (anchor point) representing maximum compaction for practical purposes; i.e., the porosity estimated at a depth of 4 km ( $\phi_{4\text{km}}$ ,  $V_{4\text{km}}$ ) (Table 1a; curve  $V_N^{ss10}$  in Figure 3a). We calculate rock properties for consolidated sandstones with clay contents of 0, 10, 20 and 30%, using  $\phi_{4\text{km}} = 17.6\%$ , from Han's empirical relations based on a data set with mean porosity 16% (Table 1b) (Han et al. 1986).

This modified Voigt model is appropriate where data extend over depths ranging from partially consolidated, shallow rocks to deeper, well consolidated rocks. In such situations diagenesis is the dominant control over the  $V$ - $\phi$  trend, and the modified Voigt model seems to capture this behaviour. However, in cases where data all come from similar diagenetic ages, such as from a selected reservoir zone within a relatively narrow depth range, variations in texture, sorting, and clay content dominate the  $V$ - $\phi$  trend, and models other than the modified Voigt are more appropriate (e.g. Dvorkin and Nur 1996).

### ***$\phi$ - $z$ model***

Sclater and Christie (1980) suggested an exponential porosity-depth trend for sandstones in the North Sea, constrained by a surface porosity of 49% estimated for sand in Holocene beach and dune deposits by Pryor (1973). This value is above the surface value of 41% for river bar sediments given by Pryor, and above the critical porosity for clean and well sorted sand,  $\phi_c=40\%$  (Nur et al. 1998). Further, a surface porosity of 44% for sandstones was found by fitting an exponential decay function with porosities based on density log data (Serra 1986). Both trends, however, indicate similar

porosities at depth, i.e., a mean value of  $\phi_{4\text{km}}=17.6\%$ . We calculate the exponential decay constant ( $\beta$  in equation 2) for that value and  $\phi_0=40\%$ , and do not include the influence of clay content (Figure 3b; Table 1a).

### ***Resulting V-z model***

V-z trends for sandstone are found by eliminating  $\phi$  from the above two models (curve  $V_N^{ss30}$  in Figure 3c; equations A-2 and 2). The modified Voigt model defined by the minimum-porosity anchor point has a V-z gradient that decreases monotonously from values greater than  $1 \text{ s}^{-1}$  for  $z<0.4 \text{ km}$  and 30% clay content (Figure 3d; Table 1c).

Reduction of the clay content leads to higher velocity and velocity gradient (Figure 9).

We can approximate the modified Voigt model by a modified velocity-average equation (equation B-2).

If we compare the modified Voigt model with the normal trend for the Bunter Shale and Sandstone (Figures 6, 7), we see that the Bunter trend – and most data points corrected for exhumation – plot between the sandstone models for 0% and 10% clay content for depths below *c.* 2 km. The match between the modified Voigt model and the data points for the Bunter Sandstone supports the application of the modified Voigt model for sandstone (Figure 3) as well as the estimation of the amount of exhumation by means of chalk velocities (Figure 5).

The match between the modified Voigt model and the data points for the Bunter Shale suggests that the lithology of the Bunter Shale is dominated by quartz in the wide area covered by the data set (southern and eastern North Sea Basin). Consequently, the term ‘Shale’ seems to be an indication of grain size rather than of mineralogy.

The low velocities of the Bunter trend relative to the modified Voigt model at shallow depths model may be explained by slow porosity reduction in the Bunter Shale

and Sandstone due to mechanical compaction above *c.* 2 km followed by a more rapid reduction due to the onset of quartz cementation below that depth (cf. Bjørlykke and Egebjerg 1993; Lander and Walderhaug 1999).

The velocity-depth relations for the Triassic Bunter Sandstone established by Bulat and Stoker (1987), and by Hillis (1995) predict velocities at intermediate depths that are in agreement with the modified Voigt model for sandstone with 10% clay (e.g.  $z \approx 2$  km; curves *B&S*, *H* and  $V_N^{ss10}$ , in Figure 10a). However, only the modified Voigt model complies with reasonable boundary conditions at the surface and at infinite depth (Figure 10b). In contrast, the Bunter Sandstone model of Hillis (1995) predicts that the velocity-depth gradient increases towards infinity (cf. equation C-2). Consequently, exhumation may be underestimated by more than 500 m when this unconstrained sandstone trend is applied for velocities greater than 3.7 km/s compared to the modified Voigt model presented here. Underestimation by such amounts, which is only due to an unconstrained formulation of the baseline, is considerable compared to e.g. the amount of Cenozoic exhumation of the North Sea Basin that reaches *c.* 1 km where the Upper Cretaceous Chalk is truncated (Japsen 1998, 2000).

### **V- $\phi$ -z relations for shale**

#### ***V- $\phi$ model***

Hansen (1996a) calculated porosities from grain densities measured on cuttings and sidewall cores and from bulk densities estimated from density logs for Cretaceous-Cenozoic shales in three wells on the Norwegian Shelf. Corresponding transit times were determined by averaging sonic log values near the sampling depth. A modification of the Wyllie et al. (1956) time-average equation yielded a good fit for this data set

(Figure 4a) (Hansen 1996a). The modified time-average equation is in the form of equation (B-1) where  $1/\phi_c$  is substituted by a correction factor,  $C_P$ . Hansen (1996a) found  $C_P=1.57$  ( $\phi_c=64\%$ ;  $V_c=1610$  m/s;  $V_m=5155$  m/s), and

$$tt = 670 \cdot \phi + 194 . \quad (6)$$

According to Hansen (1996a) differences in the determination of shale porosity are the main causes for differences between this result and the  $V$ - $\phi$  relations for shale of Magara (1976), Issler (1992), and Liu and Roaldset (1994).

### ***$\phi$ -z model***

Hansen (1996a) calculated shale porosities from transit times based on the above  $tt$ - $\phi$  relation for normally compacted Cretaceous-Cenozoic shale intervals in 29 wells on the Norwegian Shelf. Exponential and linear  $\phi$ -z trends were fitted to the data, giving  $\phi_0=71\%$  and  $62\%$ , respectively, which is in reasonable agreement with  $\phi_c=64\%$  indirectly determined by equation (6) (Figure 4b; Table 1a).

### ***Resulting V-z model***

The expression resulting from combining the  $V$ - $\phi$  trend of equation (6) with the suggested exponential  $\phi$ -z relation (Hansen 1996a; Table 1a) is a constrained, transit time-depth model (equation C-5; curve 1 in Figure 4c):

$$tt = 476 \cdot e^{-z/1961} + 194 . \quad (7)$$

Hansen (1996b), however, chose to fit a simple, transit time-depth model (equation C-3) to data from normally compacted Jurassic-Miocene shale intervals in 32 wells on the Norwegian Shelf ( $0.4 < z < 2.8$  km):

$$tt = 627 \cdot e^{-z/3704} . \quad (8)$$

This equation predicts velocity to approach infinity at depth, and the two above trends are 0.8 km apart for  $V=4$  km/s (curve  $Ha$  in Figure 4c). By contrast, the shale trend of Japsen (2000) given by equation (5) (curve  $V_N^{sh}$  in Figure 4d, Table 1c) is almost identical to that given by equation (7). Furthermore, it is less than 100 m apart from the trend of Hansen (1996b) for  $z < 2.4$  km which is the interval that covers most of the Cenozoic shale data.

Scherbaum (1982) presented a baseline for Lower Jurassic shale in the Northwest German Basin, and this trend is within 100 m from that given by equation (5) for the adjacent Danish Basin for  $z < 4$  km. Corcoran and Mecklenburgh (2005) estimated a shale trend of the same form as equation (5) based on regression of sonic log data for normally compacted, Jurassic-Cenozoic shale in the Rockall and Porcupine basins. Inclusion of data from non-shale sediments in the analysis of Corcoran and Mecklenburgh (2005) may have caused their trend to be on average 497 m more shallow than the trend given by equation (5) for a given velocity and  $z < 4$  km. Uncertainty is thus related to identifying a uniform lithology for which the baseline is defined and to selecting data for similar formations for which exhumation is to be determined. Shale trends based on data from the Gulf Coast area match that given by equation (5) at intermediate depths from where most of the Cenozoic shale data originate ( $0.5 < z < 1.5$  km). Few details are, however, given about the derivation of the Gulf Coast shale trends (e.g. Hottmann and Johnson 1965; Chapman 1983).

### **Overpressure-prediction from shale velocities**

Overpressure in the central North Sea was successfully predicted from velocity-depth anomalies for the Cenozoic succession relative to a normal velocity-depth trend for shale close to that given by equation (5) (Figure 11; Japsen 1999). Investigation of

interval velocities from almost a thousand wells revealed basin-wide differences in the physical properties of the Cenozoic deposits related to disequilibrium compaction below the mid-Miocene unconformity in the central North Sea (cf. Rubey and Hubbert 1959; Osborne and Swarbrick 1997).

The overpressure of an undercompacted rock,  $\Delta P_{comp}$ , is proportional to the burial anomaly,  $dZ_B$  [m] (Figure 1):

$$\Delta P_{comp} \approx dZ_B/100 \text{ [MPa]}, \quad (9)$$

which means that a burial anomaly of 1000 m may reflect overpressure due to undercompaction of 10 MPa (Japsen 1998). In Figure 11c we compare the degree of undercompaction of the lower Cenozoic succession in the North Sea expressed by its burial anomaly,  $dZ_B^{low}$ , with pressure data from the underlying Chalk,  $\Delta P_{Ch}$ , because pressure measurements from the lower Cenozoic shales are rare in the central North Sea. We observe that  $\Delta P_{Ch}$  is proportional to  $dZ_B^{low}$ , and in the order of the overpressure predicted by equation (9). This indicates that the burial anomaly for the lower Cenozoic succession relative to the shale trend given by equation (5) is a measure of overpressure due to undercompaction.

### **Comparison of $V$ - $z$ models for sandstone and shale**

The velocity at the surface varies little for the sandstone and shale models presented here (c. 1.6 km/s; Table 1c; Figure 9). However, different velocity gradients during normal compaction lead to a considerable range of velocities at a burial depth of 1 km for these models: Sandstone velocities range from 2.6 to 3.1 km/s (30 to 0% clay content), while that of shale is predicted to be 2.1 km/s. For the models in the Figure we predict the velocity of marine shale to be lower than that for sandstone with a clay

content below 30% for  $z < 3.5$  km.

The shapes of the velocity-depth trends for sandstone and shale differ markedly at shallow depth as indicated by the much higher velocity gradient for sandstone than for shale ( $1-1.5 \text{ s}^{-1}$  as opposed to  $0.55 \text{ s}^{-1}$ , respectively, for  $z$  increasing from 0 to 1 km).

Whereas the gradient for the sandstone trends decreases monotonously with depth, that for shale has a maximum value of  $0.62 \text{ s}^{-1}$  for  $z=2.0$  km. However, the velocity gradients are all close to  $0.5 \text{ s}^{-1}$  for the sandstone and shale models at intermediate depths.

## **DISCUSSION**

Identification of a normal velocity-depth trend from basinwide well data involves three steps of generalization, and this may explain differences among trends suggested for identical units by different authors. First, the model should be established for formations that are relatively homogenous with regards to macroscopic acoustic properties; e.g. sandstone units of equal clay content or marine shale dominated by smectite/illite. Second, the trend should reflect normal compaction, but burial anomalies of  $\pm 1$  km relative to the trend may be expected as the result of over- and undercompaction (Figures 1, 11). Third, the mathematical formulation of the normal velocity-depth trends should be constrained by knowledge from rock physics.

Unconstrained trend lines fitted to local velocity-depth data may be useful for estimating onset of overpressure or for predicting velocity within a limited depth range. However, a normal velocity-depth trend that complies with the above criteria is a prerequisite for estimating absolute values of depth, overpressure and the amount of exhumation based on sonic data for a sedimentary formation. Estimates of previous depth of burial (and hence exhumation) should thus be based on velocity data and models for specific lithologies: depth of normal compaction varies by more than 1 km

depending on whether the lithology is assumed to be shale or pure sandstone for e.g.  $V=3$  km/s (Figure 9). Consequently, the constrained, exponential  $tt-z$  trend given by equation (C-5) that implies a  $V-\phi$  relation characteristic of a marine shale should not be applied to sand/shale series (e.g., Heasler and Kharitonova 1996) nor to Triassic redbeds (e.g. Ware and Turner 2002) (see Appendix B).

Normal compaction may be a difficult condition to prove because we do not always know if formation pressure is hydrostatic (e.g. in shale) or if a formation has been buried deeper prior to exhumation. If for instance a formation is exhumed, the observed minimum velocity at the surface may be mistaken for the normal velocity of the formation at zero depth prior to burial. These effects led Faust (1951) to suggest that the velocity for sand-shale sections was proportional to  $(zT)^{1/6}$ , where  $T$  is geologic time in years (compare equation C-4). Acheson (1963), however, realized that the apparent age effect observed by Faust could be explained by exhumation.

Japsen (1999) suggested that a shale trend close to that given by equation (5) could be applied more widely to marine shale dominated by smectite/illite and thus possibly to the Cenozoic shales in e.g. the Gulf Coast area. Illite and smectite are the main components of marine shale, and make up 70% of the clay minerals in the major ocean basins today, and the shale of the Cenozoic deposits of the North Sea Basin and in the Gulf Coast area is also dominated by smectite/illite (Weaver 1989). The validity of the baseline for marine shale given by equation (5) is indicated firstly by the successful prediction of overpressure in the North Sea (Figure 11), secondly by the correspondence between this baseline and other suggested shale lines over significant velocity ranges (Scherbaum 1982; Hansen 1996b) and finally, by the fact that the trend is constrained by  $V-\phi-z$  relations for shale (Figure 4).

## CONCLUSIONS

The formulation of a normal velocity-depth trend for a formation is not an arbitrary choice of mathematical functions and regression parameters. The trend should be considered as a physical model of how the sonic velocity of a given lithology increases as porosity is reduced during burial and normal compaction in a sedimentary basin. We have investigated the properties of normal velocity-depth trends for sandstone and shale by combining typical  $V$ - $\phi$  trajectories and exponential  $\phi$ - $z$  relations that are constrained by the critical porosity of the sediment at the surface and have shown that:

- The concave  $V$ - $\phi$  path for sandstone with initial grain contact leads to a monotonous decrease of the velocity gradient with depth. Therefore,  $V$ - $z$  trends for consolidated sandstone have often been approximated by power-law  $V$ - $z$  trends with the velocity gradient decreasing monotonously with depth, a formulation that predicts zero velocity at the surface and infinite velocity at depth. We present a constrained  $V$ - $z$  trend for sandstone based on a modified Voigt model (equation A-2), and – as an approximation to this trend – a constrained, exponential  $V$ - $z$  trend based on a modified velocity-average equation (equation B-2).
- The convex  $V$ - $\phi$  path of lithologies such as shale or chalk that are initially compliant may lead to a maximum velocity gradient at some intermediate depth before the gradient approaches zero.  $V$ - $z$  trends for marine shale have thus often been approximated by exponential  $tt$ - $z$  trends for which the velocity gradient increases (towards infinity) with depth. We suggest a constrained, exponential  $tt$ - $z$  model (equation 5) based on a modified time-average equation (equation B-1), as other workers have done before us.

The case study of baselines for sandstone and shale in the North Sea underlines the importance of applying constrained models and also the difficulty of estimating such trends when the sediments are not at maximum burial due to exhumation. The baseline for the redbeds of the Triassic Bunter Shale and Sandstone is found to be in agreement with the modified Voigt model for sandstone assuming that the onset of quartz cementation occurs below a depth of c. 2 km. The baseline for marine shale agrees with the shale trends of previous workers, and it can be applied to predict overpressure from sonic data.

Normal velocity-depth trends derived from basinwide data thus give us the opportunity to study the rock physical behaviour of different lithologies under natural conditions that may be difficult to imitate in a laboratory.

## **ACKNOWLEDGEMENTS**

The financial support from the Carlsberg Foundation, GEUS and Stanford Rock and Borehole Geophysics Project is gratefully acknowledged. The constructive comments of reviewers, editors, J.A. Chalmers and J. Ineson improved the paper.

## **REFERENCES**

- Acheson, C.H. 1963. Time-depth and velocity-depth relations in western Canada. *Geophysics* **28**, 894–909.
- Al-Chalabi, M. 1997a. Instantaneous slowness versus depth functions. *Geophysics* **62**, 270–273.
- 1997b. Time-depth relationships for multilayer depth conversion. *Geophysical Prospecting* **45**, 715–720.
- Athy, L.F. 1930. Compaction and oil migration. *American Association of Petroleum*

*Geologists Bulletin* **14**, 25–35.

Bertelsen, F. 1980. *Lithostratigraphy and depositional history of the Danish Triassic*.

Geological Survey of Denmark. Series B, 4. Geological Survey of Denmark.

Bjørlykke, K. and Egebjerg, P.K. 1993. Quartz cementation in sedimentary basins.

*American Association of Petroleum Geologists Bulletin* **77**, 1538–1548.

Bulat, J. and Stoker, S.J. 1987. Uplift determination from interval velocity studies, UK,

southern North Sea. In: *Petroleum geology of north west Europe* (eds J. Brooks and K.W. Glennie), pp. 293–305, Graham & Trotman.

Chapman, R.E. 1983. *Petroleum geology*. Elsevier.

Chen, Q. and Nur, A. 1994. Critical concentration models for porous materials. In:

*Advances in porous media* (ed. M.Y. Corapcioglu), pp. 169–308, Elsevier.

Corcoran, D.V. and Doré, A.G. 2005. A review of techniques for the estimation of

magnitude and timing of exhumation in offshore basins. *Earth-Science Reviews* **72**, 129–168.

Corcoran, D.V. and Mecklenburgh, R. 2005. Exhumation of the Corrib Gas Field, Slyne

Basin, offshore Ireland. *Petroleum Geoscience* **11**, 239–256.

Dvorkin, J., Gutiérrez, M.A. and Nur, A. 2002. On the universality of diagenetic trends.

*The Leading Edge*, January 2002 40–43.

Dvorkin, J. and Nur, A. 1996. Elasticity of high-porosity sandstones - theory for two

North Sea data sets. *Geophysics* **61**, 1363–1370.

Fabricius I.L. 2003. How burial diagenesis of chalk sediments controls sonic velocity

and porosity. *American Association of Petroleum Geologists Bulletin* **87**, 1755–1778.

Faust, L.Y. 1951. Seismic velocity as a function of depth and geologic time. *Geophysics*

16, 192–206.

Feng, S. and Sen, P.N. 1985. Geometrical model of conductive and dielectric properties of partially saturated rocks. *Journal of Applied Physics* **58**, 3236–3243.

Greenberg, M. L. and Castagna, J. P. 1992. Shear-wave velocity estimation in porous rocks: Theoretical formulation, preliminary verification and applications, *Geophysical Prospecting*, **40**, 195–209.

Guéguen, Y. Chelidze, T. and Le-Ravalec, M. 1997. Microstructures, percolation thresholds, and rock physical properties. *Tectonophysics* **279**, 1–4, 23–35.

Guéguen, Y. and Palciauskas, V. 1994. *Introduction to the physics of rocks*. Princeton University Press.

Han, D.H. Nur, A. and Morgan, D. 1986. Effects of porosity and clay content on wave velocities in sandstones. *Geophysics* **51**, 2093–2107.

Hansen, S. 1996a. A compaction trend for Cretaceous and Tertiary shales on the Norwegian Shelf based on sonic transit times. *Petroleum Geoscience* **2**, 159–166.

-----1996b. Quantification of net uplift and erosion on the Norwegian Shelf south of 66°N from sonic transit times of shale. *Norsk Geologisk Tidsskrift* **76**, 245–252.

Haskell, N.A. 1941. The relation between depth, lithology, and seismic wave velocity in Tertiary sandstones and shales. *Geophysics* **6**, 318–326.

Heasler, H.P. and Kharitonova, N.A. 1996. Analysis of sonic well logs applied to erosion estimates in the Bighorn Basin, Wyoming. *American Association of Petroleum Geologists Bulletin* **80**, 630–646.

Hillis, R.R. 1995. Quantification of Tertiary exhumation in the United Kingdom southern North Sea using sonic velocity data. *American Association of Petroleum*

*Geologists Bulletin* **79**, 130–152.

Hottmann, C.E. and Johnson, R.K. 1965. Estimation of formation pressures from log-derived shale properties. *Journal of Petroleum Technology* **17**, 717–723.

Issler, D.R. 1992. A new approach to shale compaction and stratigraphic restoration, Beaufort-Mackenzie Basin and Mackenzie Corridor, northern Canada. *American Association of Petroleum Geologists Bulletin* **76**, 1170–1189.

Japsen, P. 1993. Influence of lithology and Neogene uplift on seismic velocities in Denmark; implications for depth conversion of maps. *American Association of Petroleum Geologists Bulletin* **77**, 194–211.

-----1998. Regional velocity-depth anomalies, North Sea Chalk. A record of overpressure and Neogene uplift and erosion. *American Association of Petroleum Geologists Bulletin* **82**, 2031–2074.

-----1999. Overpressured Cenozoic shale mapped from velocity anomalies relative to a baseline for marine shale, North Sea. *Petroleum Geoscience* **5**, 321–336.

-----2000. Investigation of multi-phase erosion using reconstructed shale trends based on sonic data. Sole Pit axis, North Sea. *Global and Planetary Change* **24**, 189–210.

Johnson, H., Warrington, G. and Stoker, S.J. 1994. 6. Permian and Triassic of the southern North Sea. In: *Lithostratigraphic nomenclature of the UK North Sea* (eds R.W. O'B. Knox and W.G. Cordey. British Geological Survey.

Lander, R.H. and Walderhaug, O. 1999. Predicting porosity through simulating sandstone compaction and quartz cementation. *American Association of Petroleum Geologists Bulletin* **83**, 433–449.

Liu, G. and Roaldset, R. 1994. A new decompaction model and its application to the

- northern North Sea. *First Break* **12**, no. 2, 81–89.
- Magara, K. 1976. Thickness of removed sedimentary rocks, paleopore pressure, and paleotemperature, southwestern part of Western Canada Basin. *American Association of Petroleum Geologists Bulletin* **60**, 554–565.
- Magara, K. 1978. *Compaction and fluid migration. Practical petroleum geology*. Elsevier.
- Marion, D. Nur, A. Yin, H. and Han, D. 1992. Compressional velocity and porosity in sand-clay mixtures. *Geophysics* **57**, 554–563.
- Mavko, G., Mukerji, T. and Dvorkin, J. 1998. *The rock physics handbook*. Cambridge University Press.
- Michelsen, O., 1989. *Revision of the Jurassic lithostratigraphy of the Danish subbasin*. Geological Survey of Denmark, Copenhagen.
- Nolen-Hoeksema, R.C. 1993. Porosity and consolidation limits of sediments and Gassmann's elastic-wave equation. *Geophysical Research Letters* **20**, 847–850.
- Nur, A., Marion, D. and Yin, H. 1991. Wave velocities in sediments, In: *Shear waves in marine sediments* (ed. J.M. Hovem) pp. 131–140, Kluwer Academic Publishers.
- Nur, A., Mavko, G., Dvorkin, J. and Galmundi, D. 1998. Critical porosity; a key to relating physical properties to porosity in rocks. *Leading Edge* **17**, 357–362.
- Olsen, R.C., 1979, *Lithology. Well 17/10-1*. NPD Paper 21.
- Osborne, M.J. and Swarbrick, R.E. 1997. Mechanisms for generating overpressure in sedimentary basins. A reevaluation. *American Association of Petroleum Geologists Bulletin* **81**, 1023–1041.
- Pryor, W.A. 1973. Permeability-porosity patterns and variations in some Holocene sand bodies. *American Association of Petroleum Geologists Bulletin* **57**, 162–189.

- Raymer, L.L., Hunt, E.R. and Gardner, J.S. 1980. An improved sonic transit time-to-porosity transform, in *SPWLA 21 Annual Logging Symposium, July 8–11, 1980*, 1–12.
- Rolle, F. 1985. Late Cretaceous-Tertiary sediments offshore central West Greenland. lithostratigraphy, sedimentary evolution, and petroleum potential. *Canadian Journal of Earth Science* **22**, 1001–1019.
- Rubey, W.W. and Hubbert, M.K. 1959. Role of fluid pressure in mechanics of overthrust faulting, II. *Geological Society of America Bulletin* **70**, 167–206.
- Scherbaum, F. 1982. Seismic velocities in sedimentary rocks; indicators of subsidence and uplift. *Geologische Rundschau* **71**, 519–536.
- Scholle, P.A. 1977. Chalk diagenesis and its relation to petroleum exploration; oil from chalks, a modern miracle? *American Association of Petroleum Geologists Bulletin* **61**, 982–1009.
- Slater, J.G. and Christie, P.A.F. 1980. Continental stretching; an explanation of the post-Mid-Cretaceous subsidence of the central North Sea basin. *Journal of Geophysical Research* **85**, 3711–3739.
- Serra, O. 1986. *Fundamentals of well-log interpretation*. Elsevier.
- Slotnick, M.M. 1936. On seismic computations, with applications, II. *Geophysics* **1**, 299–305.
- Smith, T. and Sondergeld, C.H., 2001. Examination of AVO response in the eastern deepwater Gulf of Mexico. *Geophysics* **66**, 1864–1876.
- Snieder, R., Xie, M.Y., Pica, A. and Tarantola, A. 1989. Retrieving both the impedance contrast and background velocity. A global strategy for the seismic reflection

problem. *Geophysics* **54**, 991–1000.

Terzaghi, K. and Peck, R.P. 1968. Soil mechanics in engineering practice. John Wiley and Sons.

Ware P. D., Turner J. P. 2002. Sonic velocity analysis of the Tertiary denudation of the Irish Sea basin. In: *Exhumation of the North Atlantic Margin: Timing, Mechanisms and Implications for Petroleum Exploration*, Vol. 196 (eds. A. G. Doré, J. A. Cartwright, M. S. Stoker, J. P. Turner, N. White), pp. 355–370. Geological Society.

Weaver, C.E. 1989. *Clays, muds and shales*. Elsevier.

Winthagen P. L. A. and Verweij J. M. 2003. Estimating regional pore pressure distribution using 3D seismic velocities in the Dutch Central North Sea Graben. *Journal of Geochemical Exploration* **78-79**, 203–207.

Wyllie, M.R.J. Gregory, A.R. Gardner, L.W. 1956. Elastic wave velocities in heterogeneous and porous media. *Geophysics* **21**, 41–70.

## APPENDIX A. BOUNDS ON VELOCITY

The simplest bounds on velocity are the Voigt and Reuss bounds (c.f. Mavko et al. 1998). The Voigt upper bound of the effective elastic modulus,  $M_V$ , of  $N$  phases is

$$M_V = \sum_{i=1}^N f_i M_i,$$

where  $f_i$  is the volume fraction, and  $M_i$  is the elastic modulus of the  $i$ 'th phase (either bulk modulus [GPa],  $K = \rho(V_p^2 - 4/3 \cdot V_s^2)$ , P-wave modulus,  $M = \rho V_p^2$ , or shear modulus,  $\mu = \rho V_s^2$ ; where density of the rock is  $\rho = (1-\phi)\rho_m + \phi\rho_{fl}$  [g/cm<sup>3</sup>];  $\rho_m$  is density of the mineral material,  $\rho_{fl}$  is the fluid density;  $V_P$ ,  $V_S$  are the P- and S-wave velocities

[km/s]). The Reuss lower bound of the effective elastic modulus,  $M_R$  is

$$M \quad \frac{1}{M_R} = \sum_{i=1}^N f_i \frac{1}{M_i} .$$

The Reuss average describes exactly the effective moduli of a suspension of solid grains in a fluid. In the suspension domain,  $\phi > \phi_c$ , the effective bulk and shear moduli can be estimated quite accurately using the Reuss (iso-stress) average:

$$K_R^{-1} = (1 - \phi)K_m^{-1} + \phi K_{fl}^{-1}; \quad \mu_R = 0, \quad (\text{A-1})$$

where  $K_m$  and  $K_{fl}$  are the bulk moduli of the mineral material and the fluid. The effective shear modulus of the suspension is zero, because the shear modulus of the fluid is zero. We can thus calculate the P-wave velocity,  $V_c$ , at  $\phi_c$  where the mineral grains are barely touching ( $\mu_c=0$ ):

$$V_c = \sqrt{(K_c + 4/3 \cdot \mu_c) / \rho_c} = \sqrt{K_c / \rho_c}$$

where subscript c indicates the value at critical porosity:  $K_c^{-1} = (1 - \phi_c)K_m^{-1} + \phi_c K_{fl}^{-1}$  and  $\rho_c = (1 - \phi_c)\rho_m + \phi_c \rho_{fl}$ .

A linear trend of  $\rho V^2$  versus  $\phi$ , may be used to describe the compaction trend for clean sandstones at high effective pressure, and this leads to convenient mathematical properties (Nur et al. 1991; Marion et al. 1992). This linear dependence can be thought of as a modified Voigt average:

$$M_{MV} = (1 - \phi')M_m + \phi' M_c, \quad (\text{A-2})$$

where  $M_m$  and  $M_c$  are the moduli (bulk or shear) of the mineral material at zero porosity and of the suspension at the critical porosity ( $M_c$  is given by equation (A-1) with  $\phi=\phi_c$ ).

The expression is modified in the sense that the porosity is scaled by the critical

porosity,  $\phi' = \phi / \phi_c$ , so that  $\phi'$  ranges from 0 to 1 as  $\phi$  ranges from 0 to  $\phi_c$ . If the low porosity end-member is taken as the porosity at finite depth,  $\phi_{fin}$ , rather than 0 to fit data from sedimentary basins,  $\phi' = (\phi - \phi_{fin}) / (\phi_c - \phi_{fin})$ . Note that using the suspension modulus  $M_c$  in this form automatically incorporates the effect of pore fluids on the modified Voigt average. The modified Voigt average (equation A-2) can be transformed into a velocity-depth model by calculating porosity as a function of depth by assuming exponential porosity decay (equation 2). The appropriate rock physical properties for sandstone with 0, 10, 20 and 30% clay content based on data from Han et al. (1986) are given in Table 1b and the  $\phi$ -z model for sandstone in Table 1a.

## APPENDIX B. V-Z RELATIONS FOR SPECIFIC V- $\phi$ TRENDS

### Transit time proportional to $\phi^{\alpha_t}$ (modified time-average equation)

Let transit time be dependent on porosity raised to the power of a positive constant,  $\alpha_t$ :

$$tt = (tt_c - tt_m) \left( \frac{\phi}{\phi_c} \right)^{\alpha_t} + tt_m \Rightarrow \ln \left( \frac{tt - tt_m}{tt_c - tt_m} \right) = \alpha_t \ln \left( \frac{\phi}{\phi_c} \right),$$

where  $tt_m$  is the transit time of the matrix, and  $tt_c$  is that of the rock at critical porosity (the simple time-average for a rock is given by  $(1-\phi)tt_m + \phi tt_{fl}$ ). We see that transit time varies between  $tt_c$  and  $tt_m$  for  $\phi$  varying between  $\phi_c$  and 0%, and that  $(tt - tt_m)$  and  $\phi$  plot as a straight line on a log-log plot. The V- $\phi$  path for this relationship is convex for all positive values of  $\alpha_t$ . We get a linear  $\ln(tt - tt_m)$ -z function similar to equation (C-5) by substituting the exponential  $\phi$ -z function with decay rate  $\beta$  (equation 2):

$$tt = (tt_c - tt_m) e^{-z/b_2} + tt_m \Rightarrow \ln(tt - tt_m) = \ln(tt_c - tt_m) - \frac{z}{b_2},$$

where  $b_2 = \beta/\alpha_t$ . Conversely, we see that the above  $V$ - $z$  trend implies that transit time is proportional to  $(\phi/\phi_c)^{\beta/b_2}$  if porosity decays exponentially with depth.

If the decay rates of  $\phi$  and  $tt$  are identical,  $\beta = b_2$ , we have linearity between  $tt$  and  $\phi$  ( $\alpha_t = 1$ ), and we get a modified time-average equation:

$$tt = (tt_c - tt_m) \cdot \phi / \phi_c + tt_m . \quad (\text{B-1})$$

This equation should be compared to the Wyllie et al. (1956) time-average equation that states proportionality between transit time and porosity ( $tt_{fl}$  is the transit time of the pore fluid):

$$tt = (tt_{fl} - tt_m) \phi + tt_m ,$$

where  $\phi = 1$  is taken as maximum porosity (and not  $\phi_c$ ), and the velocity at maximum porosity equals  $V_{fl}$  (and not  $V_c$ ) (equation A-1). The constrained, transit time-depth trend of equation (C-5) can thus be derived by combining the modified time-average equation with the assumption of exponential decay of porosity (equations B-1, 2).

### **Velocity proportional to $\phi^{\alpha_v}$ (modified velocity-average equation)**

Let velocity be dependent on porosity raised to the power of a positive constant,  $\alpha_v$ :

$$V = V_m - (V_m - V_c) \left( \frac{\phi}{\phi_c} \right)^{\alpha_v} , \Rightarrow \ln(V_m - V) = \ln(V_m - V_c) + \alpha_v \ln \left( \frac{\phi}{\phi_c} \right) ,$$

where  $V_m$  is the velocity of the matrix, and  $V_c$  is that of the rock at critical porosity (the simple velocity-average for a rock is defined as  $(1-\phi)V_m + \phi V_{fl}$ ). We see that velocity varies between  $V_c$  and  $V_m$  for  $\phi$  varying between  $\phi_c$  and 0%, and that  $(V_m - V)$  and  $\phi$  plot as a straight line in a log-log plot. The  $V$ - $\phi$  path is concave for  $\alpha_v > 1$  ( $d^2V/d\phi^2 < 0$ ), and convex for  $0 < \alpha_v < 1$  while it is a straight line for  $\alpha_v = 1$  (a modified velocity-average). We

get the following linear  $\ln(V_m - V)$ - $z$  trend by substituting the exponential  $\phi$ - $z$  function with decay rate  $\beta$  (equation 2):

$$V = V_m - (V_m - V_c)e^{-z/b_3}, \Rightarrow \ln(V_m - V) = \ln(V_m - V_c) - \frac{z}{b_3}, \quad (\text{B-2})$$

where  $b_3 = \beta/\alpha_v$ . In the special case where  $\alpha_v = 1$ , velocity becomes linearly proportional to porosity, and  $b_3 = \beta$ . The trend is a constrained velocity-depth model for which the velocity gradient is monotonously decreasing with depth for all values of  $b_3$  and thus even for convex  $V$ - $\phi$  paths ( $0 < \alpha_v < 1$ ) there is not a maximum velocity-depth gradient at intermediate depths.

We can estimate the parameters in equation (B-2) as an approximation to the modified Voigt trend (equation A-2) for  $z < 4$  km taking  $V_c = 1600$  m/s; for sandstone with varying clay content we get

$$\begin{aligned} 0\% \text{ clay: } & V_m = 5065 \text{ m/s, } b_3 = 1923 \text{ m.} \\ 5\% \text{ clay: } & V_m = 4796 \text{ m/s, } b_3 = 1963 \text{ m.} \\ 10\% \text{ clay: } & V_m = 4526 \text{ m/s, } b_3 = 2003 \text{ m.} \\ 20\% \text{ clay: } & V_m = 4288 \text{ m/s, } b_3 = 2042 \text{ m.} \\ 30\% \text{ clay: } & V_m = 4056 \text{ m/s, } b_3 = 2076 \text{ m.} \end{aligned}$$

The depth predicted by these approximations deviates less than 90 m from the respective Voigt model for a given velocity and this is considered insignificant. The model for 5% clay corresponds to the normal velocity-depth trend for the redbeds of the Triassic Bunter Shale and Sandstone formations ( $V > 3.6$  km/s; see Figure 6, 7)

## **APPENDIX C. REVIEW OF ANALYTICAL FORMULATIONS OF V-Z TRENDS**

Several functions have been applied to represent the increase of velocity with depth

(Table 2). A linear velocity-depth function has been used by several workers for different lithologies (e.g., Slotnick 1936; Bulat and Stoker 1987; Japsen 1993).

$$V = V_0 + kz, \quad (\text{C-1})$$

where the velocity-depth gradient,  $k$ , is positive (curve *B&S* in Figure 10).

Hillis (1995) applied a linear function between transit time and depth for chalk, sandstone and shale:

$$tt = tt_0 + qz, \quad (\text{C-2})$$

where  $tt_0$  is the transit time at the surface, and  $q$  [ $\mu\text{s}/\text{m}^2$ ] is the negative transit time-depth gradient (c.f. Al-Chalabi 1997a; curve *H* in Figure 10).

Velocity-depth relations for shale have often been approximated by a simple exponential model for the reduction of transit time with depth (e.g., Hottmann and Johnson 1965; Magara 1978; Hansen 1996b):

$$tt = tt_0 e^{-z/b_1}, \Rightarrow \ln(tt) = \ln(tt_0) - z/b_1 \quad (\text{C-3})$$

where  $b_1$  [m] is an exponential decay constant (curve *Ha* in Figure 4).

Acheson (1963) found that velocity in sedimentary basins was proportional to depth raised to the power of  $(1-n)$ :

$$V = dz^{1-n}, \Rightarrow \ln(V) = \ln(d) + (1-n)\ln(z), \quad (\text{C-4})$$

where  $n$  is a number between 0.83 and 1, and  $d$  [ $\text{m}^n/\text{s}$ ] a coefficient. The velocity at the surface is predicted to be zero, so the expression is only valid below some depth.

Similar formulations was applied by Faust (1951).

The above four formulations are linear relations in the  $V$ - $z$ ,  $tt$ - $z$ ,  $\ln(tt)$ - $z$  or  $\ln(V)$ - $\ln(z)$  plane, respectively. While they may be valid approximations within a given interval, they all predict that velocity approaches infinity at depth. Only the power-law  $V$ - $z$  trend

(equation C-4) predicts the velocity gradient to decrease with depth; the linear  $V$ - $z$  trend (equation C-1) has a constant gradient, and the linear  $tt$ - $z$  and the exponential  $tt$ - $z$  trends (equations C-2 and C-3) have increasing gradients with depth. However, we have shown that an increasing velocity gradient at shallow depths characterizes initially compliant sediments, whereas the velocity gradient for initially stiff rocks decreases with depth. This point explains why the linear  $tt$ - $z$  and exponential  $tt$ - $z$  trends have been applied so successfully to initially compliant rocks, like chalk and shale (e.g., Hottmann and Johnson 1965; Hillis 1995), and why the power-law  $V$ - $z$  model primarily has been applied to sand-shale sequences (e.g., Faust 1951; Acheson 1963).

A constrained, exponential transit time-depth model was suggested for shale by Chapman (1983), and applied for sand/shale series by Heasler and Kharitonova (1996) and for Triassic redbeds by Ware and Turner (2002):

$$tt = (tt_0 - tt_\infty) e^{-z/b_2} + tt_\infty, \Rightarrow \ln(tt - tt_\infty) = -z / b_2 \cdot \ln(tt_0 - tt_\infty), \quad (\text{C-5})$$

where  $tt_\infty$  is the transit time at infinite depth, and  $b_2$  [m] is an exponential decay constant (c.f. Al-Chalabi 1997a). This model predicts finite values of transit time at the surface and at infinite depth;  $tt_0$  and  $tt_\infty$ , respectively. This formulation is linear in the  $\ln(tt - tt_\infty)$ - $z$  plane, and implies that  $k \rightarrow 0$  for  $z \rightarrow \infty$ . The velocity gradient for this  $V$ - $z$  trend has a maximum for  $z = b_2 \ln[(tt_0 - tt_\infty) / tt_\infty]$ . This model may thus be applied to initially compliant rocks as shale (e.g., Chapman 1983) or more specifically to marine shale dominated by smectite/illite (equation 5; curve  $V_N^{sh}$  Figure 4) (Japsen 1999; 2000).

Segmented linear velocity-depth functions have been suggested for the North Sea chalk (Upper Cretaceous-Danian) and for the Triassic Bunter Shale because no single

mathematical function matched the observed trends (Japsen 1998; 2000). Such continuous and non-linear functions are defined over a velocity interval divided into  $n$  segments:

$$V = V_{0i} + k_i z, \quad z_{ai} < z < z_{bi} \quad (\text{C-6})$$

where  $V_{0i}$  and  $k_i$  are the velocity at the surface and the velocity-depth gradient of the  $i$ 'th segment defined for velocities between  $V_{ai}$  and  $V_{bi}$ . The shift of the velocity gradient between the segments reflects variations in the compaction process (Japsen 1998).

## FIGURE CAPTIONS

Figure 1. Burial anomaly,  $dZ_B$  [m], relative to a normal velocity-depth trend,  $V_N$ , for a sedimentary formation. In the North Sea Basin, burial anomalies of  $\pm 1$  km for pre-Miocene formations result from late Cenozoic exhumation along basin margins and overpressuring due to rapid, late Cenozoic burial in the basin centre (c.f. Figure 11). Rapid burial and low permeability cause undercompaction and overpressure,  $\Delta P_{comp}$  [MPa], and velocities low relative to depth (positive  $dZ_B$ ) (cf. equation 9). Exhumation due to uplift reduce the overburden thickness, and cause overcompaction expressed as velocities high relative to depth (negative  $dZ_B$ ); however, post-exhumational burial,  $B_E$ , will mask the magnitude of the missing section,  $\Delta z_{miss}$ . The normalized depth,  $z_N$ , is the depth corresponding to normal compaction for the measured velocity (cf. Terzaghi's principle; Terzaghi and Peck 1968). Modified after Japsen (1998).

Figure 2. Shapes of  $V$ - $\phi$  and  $V$ - $z$  curves for sediments characterized by initially stiff or initially compliant pore space (e.g. consolidated sandstone and marine shale, Figures 3, 4). The two sediments have concave and convex  $V$ - $\phi$  trajectories, and thus  $d^2V/d\phi^2$  become negative and positive, respectively. The velocity gradient,  $k=dV/dz$ , is decreasing with depth for the first type, while it has a maximum for the other type.

(a), (c) and (e)  $V$ - $\phi$  trend and first and second derivative with respect to  $\phi$ .

(b), (d) and (f)  $V$ - $z$  trend and first and second derivative with respect to  $z$ .

Exponential  $\phi$ - $z$  relations for both sediments are given in Table 1a.

$V_N^{ss10}$ : modified Voigt model for sandstone, 10% clay content (equation A-2).  $V_N^{sh}$ : marine shale (equations 5, 6,  $V$ - $\phi$  and  $V$ - $z$  relations respectively).

Figure 3. Consolidated sandstone; relations between velocity, porosity, depth and velocity-depth gradient. A modified Voigt upper bound ( $V_N^{ss30}$ ) represents the transition from sand to sandstone during normal compaction by constraining porosity to vary between critical porosity and estimated porosity at a depth of 4 km (equation A-2) (Nur et al. 1991).

(a)  $V$ - $\phi$  trends and data points for clay content between 20 and 40% at 40 MPa confining pressure (cf. Table 1b) (Han et al. 1986).

(b)  $\phi$ - $z$  trend based on models for the North Sea and Nigeria (Table 1a).

(c)  $V$ - $z$  trends resulting from elimination of  $\phi$  in Figures (a) and (b) and sonic log covering normally compacted, Cenozoic sandstones in the Kangâmiut-1 well, offshore SW Greenland (Rolle 1985).

(d)  $k$ - $z$  trends from Figure (c).

1: linear trend from lab data. 2: modified Voigt trends from mineral properties at  $\phi=0$ .

$V_N^{ss30}$ : modified Voigt trend from lab data, 30% clay content, anchor point at  $\phi_{4\text{km}}$ .

Figure 4. Shale; relations between velocity, porosity, depth and velocity-depth gradient based on North Sea data. The constrained transit-time-depth model derived from log and core data (line 1) corresponds to a normal velocity depth trend derived from interval velocity data ( $V_N^{sh}$ ).

(a)  $V$ - $\phi$  trend based on log and core data (equation 6; Hansen 1996a).

(b)  $\phi$ - $z$  trend based on transit times converted by equation (6) (Table 1a; Hansen 1996a).

(c)  $V$ - $z$  trends and sonic log from normally compacted sediments (1.1 km Cenozoic

shale, 0.3 km mainly Mesozoic chalk and 0.8 km Mesozoic shale; Norwegian well 17/10-1; compare Olsen 1979; Hansen 1996b).

(d)  $k$ - $z$  trends from Figure (c).

1: Trend resulting from elimination of  $\phi$  in Figures (a) and (b) (equation 7). Ha: Hansen 1996b (exponential  $tt$ - $z$  trend, equation 8).  $V_N^{sh}$ : Trend for marine shale dominated by smectite/illite (equation 5; Japsen 1999; 2000).

Figure 5. Identification of a normal velocity-depth trend for shale based on data from wells where Cenozoic exhumation can be estimated from velocity-depth data for the overlying North Sea chalk. Maximum burial is assumed to have occurred during the Cenozoic for both layers.

1. Estimate the Cenozoic exhumation in each well as the burial anomaly of the chalk,  $dZ_B^{ch}$ , relative to the chalk baseline,  $V_N^{ch}$ .
2. Identify baseline,  $V_N^{sh}$ , for the shale unit by plotting velocity data versus depths corrected for exhumation as estimated by the chalk data. The shale baseline can be traced more easily because the shale was at maximum burial at more locations prior to Cenozoic exhumation.

Figure 6. Plot of interval velocity versus midpoint depth for the Lower Triassic Bunter Shale. The Bunter trend,  $V_N^B$  (equation 4), can be traced more easily if present depths are corrected for the Cenozoic exhumation in each well (Figure 5). Note the agreement between the Bunter trend and the modified Voigt model for sandstone below a depth of

c. 2 km.

(a) Present-day depth below top of sediments.

(b) Depth prior to exhumation estimated by correcting present depths by the chalk burial anomaly in each well.

One data point constrains  $V_N^B$  for a pre-exhumation depth of 5.5 km.  $V_N^{ss00}$ ,  $V_N^{ss10}$  :

Modified Voigt models for sandstone, 0-10% clay content (equation A-2). Modified after Japsen (2000).

Figure 7. Plot of interval velocity versus midpoint depth for Bunter Sandstone. The Bunter trend,  $V_N^B$  (equation 4), follows the scattered trend of the Bunter Sandstone data in the plot of depths corrected for exhumation in each well.

(a) Present-day depth below top of sediments.

(b) Depth prior to exhumation estimated by correcting present depths by the chalk burial anomaly in each well.

Three data point plot close to  $V_N^B$  for a pre-exhumation depths of c. 5 km.  $V_N^{ss00}$ ,  $V_N^{ss10}$  :

Modified Voigt models for sandstone, 0-10% clay content (equation A-2). Modified after Japsen (2000).

Figure 8. Plot of interval velocity versus midpoint depth for a marine, Lower Jurassic shale (F-1 Member of the Fjerritslev Formation). The shale trend,  $V_N^{sh}$  (equation 5), can be traced more easily if present depths are corrected for Cenozoic exhumation in each well.

(a) Present-day depth below top of sediments.

(b) Depth prior to exhumation estimated by correcting present depths by the chalk burial anomaly in each well. Modified after Japsen (2000).

Figure 9. Composite plot of normal velocity-depth trends for consolidated sandstone and shale. The velocity of shale is predicted to be lower than that predicted for sandstone with a 30% clay content for  $z < 4$  km. The velocity gradient for sandstone is predicted to be decreasing with depth whereas that of shale has a maximum at intermediate depth.

(a)  $V$ - $z$  trends.

(b)  $k$ - $z$  trends.

$V_N^{sh}$ : Marine shale (equation 5).  $V_N^{ss00}$  -  $V_N^{ss30}$ : Modified Voigt models for sandstone, 0-30% clay content (equation A-2).

Figure 10. Comparison of suggested velocity-depth trends for the Triassic Bunter Sandstone, North Sea, with the modified Voigt model for sandstone with 10% clay ( $V_N^{ss10}$ ). The two trends (B&S and H) show behaviour similar to the Voigt model at intermediate depths for which the trends were derived. Only the velocity gradient of the Voigt model converges towards zero at great depth. Data for the Bunter Sandstone are shown in Fig. 8 (cf. Japsen 2000).

(a)  $V$ - $z$  trends.

(b)  $k$ - $z$  trends.

B&S: Bulat and Stoker (1987) (linear  $V$ - $z$  trend, compare equation C-1). H: Hillis (1995) (linear  $tt$ - $z$  trend, compare equation C-2).  $V_N^{ss10}$ : modified Voigt model for sandstone, 10% clay content (equation A-2).

Figure 11. Prediction of overpressure in the North Sea from interval velocities of the Cenozoic deposits (excluding the Danian) (cf. Figure 1).

(a) Sonic log where low velocities reveal undercompaction of the lower Cenozoic sediments corresponding to measured overpressure in the underlying chalk.

(b1) and (b2) Interval velocity versus depth to the midpoint of the upper and lower Cenozoic deposits, respectively, for 322 North Sea wells.

(c) Burial anomalies for the lower Cenozoic sediments ( $dZ_B^{low}$ ) versus Chalk formation overpressure ( $\Delta P$ ) in North Sea wells.

The upper Cenozoic deposits are close to normal compaction whereas velocity-depth anomalies for the lower Cenozoic sediments outline a zone of undercompaction in the central North Sea. The deviations from the trend line in figure (c) is due to the non-compactional sources that add to the Chalk overpressure from below (transference; cf. Osborne and Swarbrick 1997), the easier drainage from the more shallow Cenozoic section and sandy lithology ( $\Delta P = dZ_B/100$ ; equation 9). The burial anomalies are calculated relative to the shale trend given by equation (5). Depths below top of sediments.  $V_N^{ss30}$ : modified Voigt model for sandstone, 30% clay content (equation A-2).  $V_N^{sh}$ : marine shale (equation 5). Modified after Japsen (1998; 1999; 2000).



**Table 1. Parameters and velocity-depth models.**

**a. Critical porosity and exponential porosity decay with depth.**

Lithology	Critical Porosity <sup>x1</sup>	Compaction models, literature				Comp.mod., applied	
		Area, depth data	$\phi_0$ [%]	$\beta$ [m]	Reference	$\phi_0$ [%]	$\beta$ [m]
Sandstone	40	North Sea, 2-3 km Nigeria, 0.6-4.3 km	49 44	3704 4631	Sclater and Christie (1980) Serra (1986)	40	4872
Shale	60-90	North Sea, 0.3-2.6 km North Sea, -	71 63	1961 1961	Hansen (1996a) Sclater and Christie (1980)	71	1961

**b. Rock physical properties.**

Material	$\phi$ [%]	$V_p$ [km/s]	$V_s$ [km/s]	$K$ [GPa]	$\mu$ [GPa]	$\rho$ [g/cm <sup>3</sup> ]	Source
Quartz	-	6.04	4.12	36.6	45.0	2.65	Mavko et al. (1998)
Water	-	1.50	0	2.25	0	1	
<b>At 4 km depth<sup>y1</sup></b>							
Sandst. 0% clay	17.6	4.66	2.95	25.1	21.6	2.48	Han et al. (1986)
Sandst. 10% clay	17.6	4.15	2.47	21.7	14.5	2.38	Han et al. (1986)
Sandst. 20% clay	17.6	3.93	2.28	20.0	12.1	2.34	Han et al. (1986)
Sandst. 30% clay	17.6	3.72	2.09	18.3	10.0	2.29	Han et al. (1986)
<b>At <math>\phi_c</math><sup>y2</sup></b>							
Quartz	40	$V_c$ 1.60	0	$K_c$ 5.15	0	$\rho_c$ 2.00	Equation (A-1)

**c. Velocity-depth models.**

V-z trend	$V_N^{ss00}$ z <sub>1</sub>	$V_N^{ss10}$ z <sub>1</sub>	$V_N^{ss20}$ z <sub>1</sub>	$V_N^{ss30}$ z <sub>1</sub>	$V_N^{sh}$ z <sub>2</sub>
$z$ [km]	$V$ [km/s]				
0	1.55	1.58	1.59	1.60	1.55
1	3.07	2.80	2.68	2.58	2.10
2	3.83	3.44	3.27	3.11	2.71
3	4.32	3.86	3.66	3.47	3.32
4	4.66	4.15	3.93	3.72	3.87
$z_i - z_{i+1}$ [km]	$k$ [s <sup>-1</sup> ]				
0-1	1.52	1.22	1.10	0.97	0.55
1-2	0.76	0.64	0.59	0.54	0.61
2-3	0.49	0.42	0.39	0.35	0.61
3-4	0.34	0.29	0.27	0.25	0.55
0-4	0.78	0.64	0.59	0.53	0.58

<sup>x1</sup> Critical porosities found by evaluation of velocity-porosity data ( Nur et al. 1998; Mavko et al. 1998).

<sup>y1</sup> Based on laboratory data and linear dependency of rock physical parameters on porosity. Porosity based on compaction models in Table 1a.

<sup>y2</sup> Reuss bound (equation A-1).

<sup>z1</sup> Sandstone model computed from the  $V-\phi$  trend given by equation A-2, the appropriate rock physical properties for 0, 10, 20 and 30% clay content (Table 1b) and the  $\phi-z$  model for sandstone (Table 1a).

<sup>z2</sup> Marine shale (equation 5).

**Table 2. Functional forms of velocity-depths trends.**

Linearity	$V(z)$ or $tt(z)$ (equation no.)	Dg · fr d. <sup>x</sup> 1	$V(0)$	$k$ $= dV/dz$	$z \rightarrow \infty$		Selected references
					$k \rightarrow$	$V \rightarrow$	
$V-z$	$V=V_0+k \cdot z$ (C-1)	2	$V_0$	$k$	$k$	$\infty$	Slotnick (1936), Bulat and Stoker (1987)
$tt-z$	$tt=tt_0+q \cdot z$ (C-2)	2	$1/tt_0$	$-q \cdot V^2$	$\infty^y$ 2	$\infty^y$ 2	Hillis (1995), Al-Chalabi (1997a)
$\ln(tt)-z$	$tt = tt_0 \cdot e^{-z/b_1}$ (C-3)	2	$1/tt_0$	$V/b_1$	$\infty$	$\infty$	Magara (1978), Hansen (1996b)
$\ln(V)-\ln(z)$	$V=c \cdot z^{1-n}$ , $0.83 < n < 1$ (C-4)	2	0	$(1-n) \cdot V/z$	0	$\infty$	Faust (1951), Acheson (1963)
$\ln(tt-tt_\infty)-z$ , $\ln(tt-tt_\infty)-\phi$ y <sup>5</sup>	$tt = (tt_0 - tt_\infty)e^{-z/b_2} + tt_\infty$ (C-5)	3	$1/tt_0$	$(V - tt_\infty \cdot V^2)/b_2$ y <sup>3</sup>	0	$1/tt_\infty$	Chapman (1983), Al-Chalabi (1997a), Japsen (1999)
$V-z$ , $N$ segments	$V=V_{0i}+k_i \cdot z$ , $z_{ai} < z < z_{bi}$ (C-6)	$2N$	$V_{0i}$	$k_i$	- y <sup>1</sup>	- y <sup>1</sup>	Japsen (1998, 2000)
$\ln(V_\infty-V)-z$ , $\ln(V_\infty-V)-$ $\ln(\phi)$ y <sup>5</sup>	$V=V_\infty-(V_\infty-V_0)e^{-z/b_3}$ (B-2) y <sup>4</sup>	3	$V_0$	$(V_\infty-V)/b_3$	0	$V_\infty$	This paper

Units of model parameters:  $b_1, b_2, b_3, z$  [m],  $c, V, V_0, V_\infty$  [m/s],  $k$  [s<sup>-1</sup>],  
 $q$  [s/m<sup>2</sup>],  $tt, tt_0, tt_\infty$  [s/m],  $z', n$  [-].

<sup>x1</sup> Degrees of freedom.

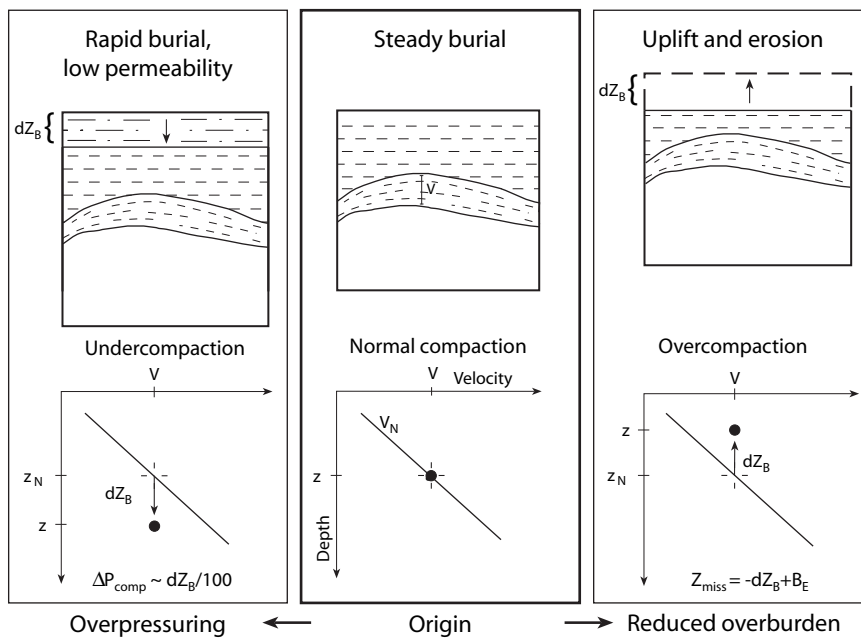
<sup>y1</sup> Arbitrary, depending on actual parameters.

<sup>y2</sup> For  $z \rightarrow -tt_0 / q$ .

<sup>y3</sup> Maximum velocity gradient for  $z = b_2 \cdot \ln[(tt_0 - tt_\infty) / tt_\infty]$ .

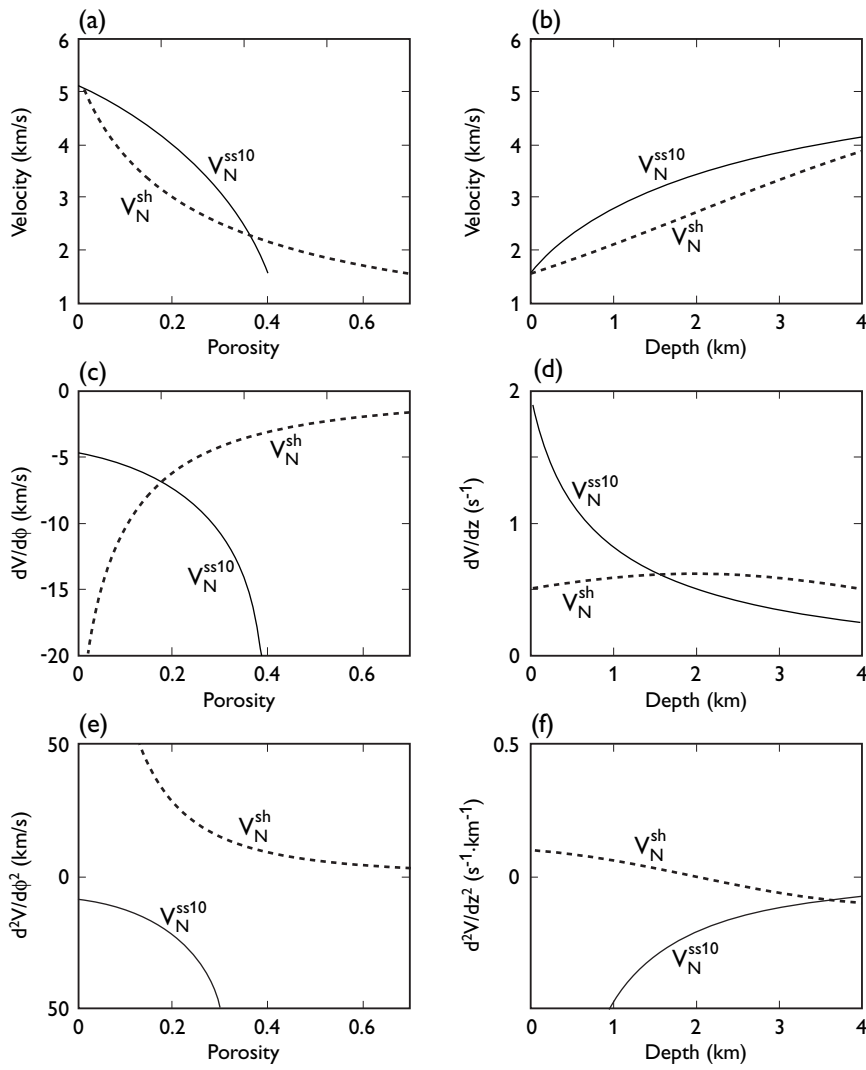
<sup>y4</sup> Constrained approximation to the modified Voigt trend based on exponential porosity-decay (equation A-2).

## Burial anomaly relative to a normal velocity-depth trend



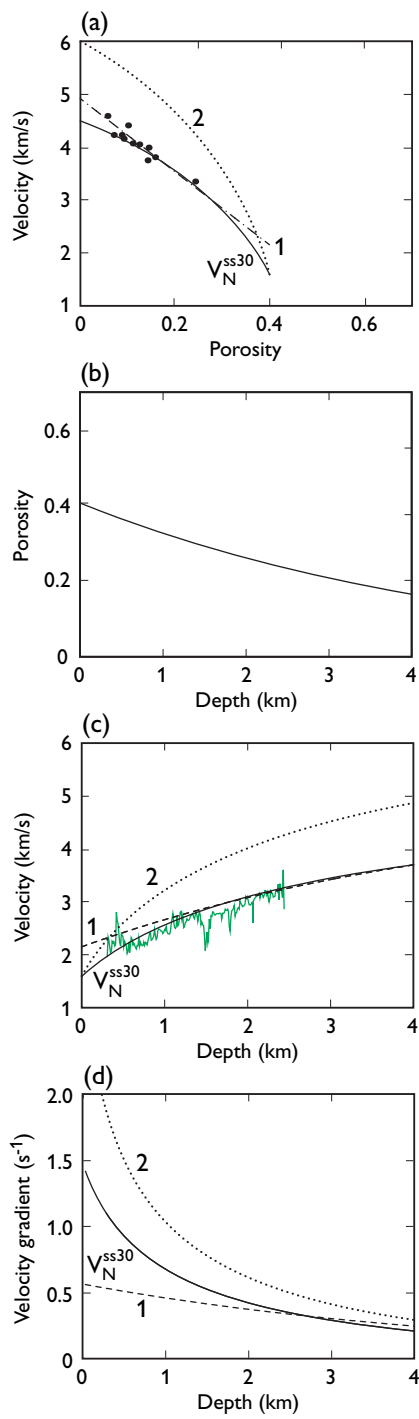
Japsen, Mukerji and Mavko, Fig.01 (1.5 column)

### Shapes of $V$ - $\phi$ and $V$ - $z$ curves



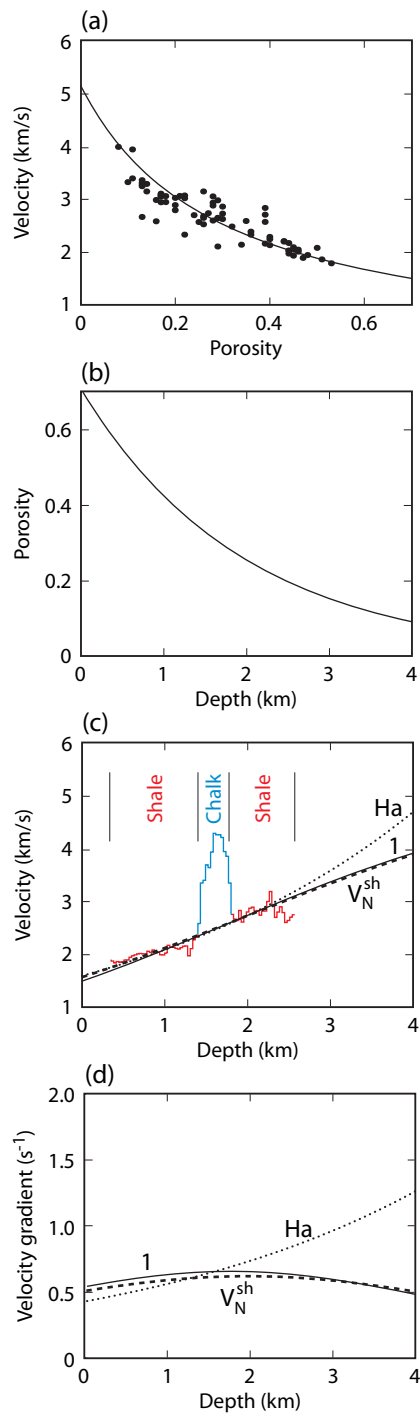
Japsen, Mukerji and Mavko, Fig.02 (1.5 column)

### V- $\phi$ -z relations for sandstone



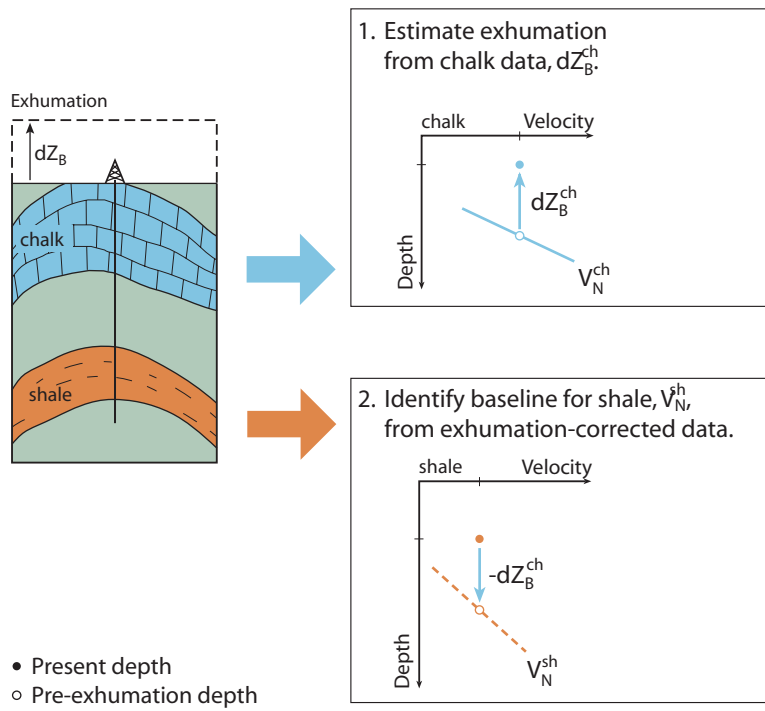
Japsen, Mukerji and Mavko, Fig.03 (1 column)

### V- $\phi$ -z relations for shale



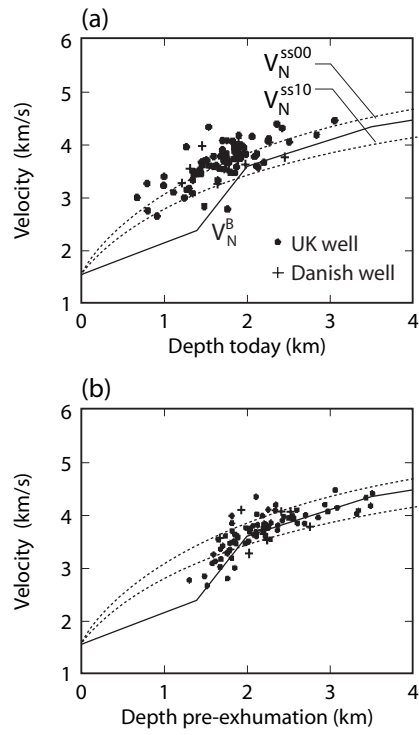
Japsen, Mukerji and Mavko, Fig.04 (1 column)

## Estimation of a baseline based on exhumation-corrected data



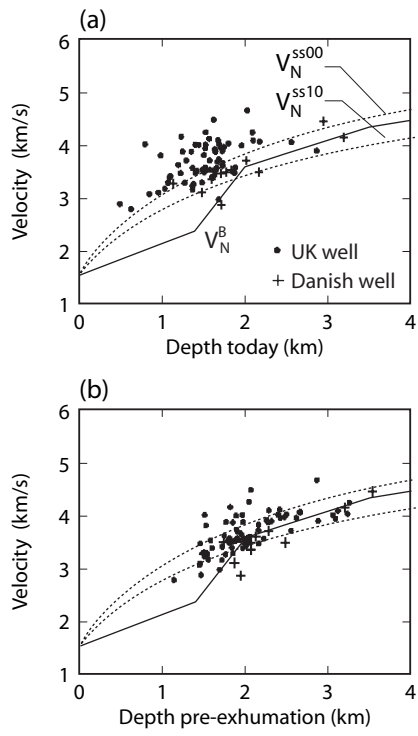
Japsen, Mukerji and Mavko, Fig.05 (1.5 column)

### Bunter Shale V-z data



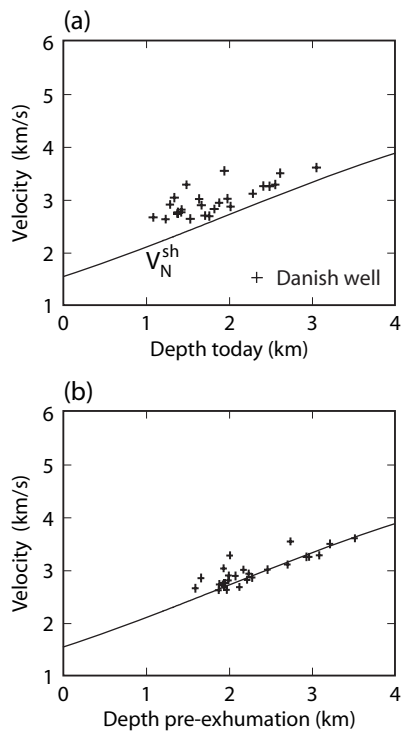
Japsen, Mukerji and Mavko, Fig.06 (1 column)

### Bunter Sandstone V-z data



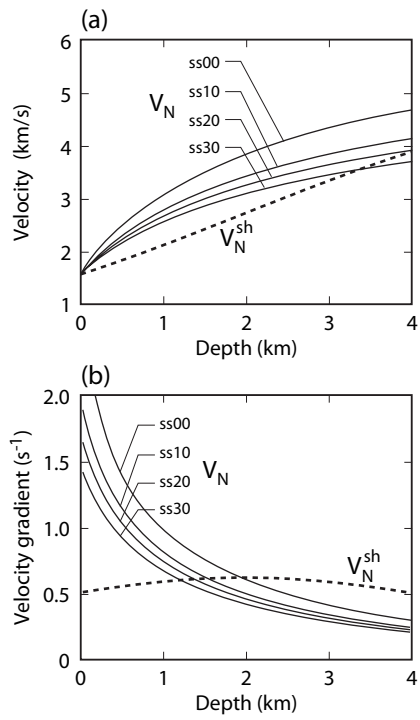
Japsen, Mukerji and Mavko, Fig.07 (1 column)

### Marine shale V-z data



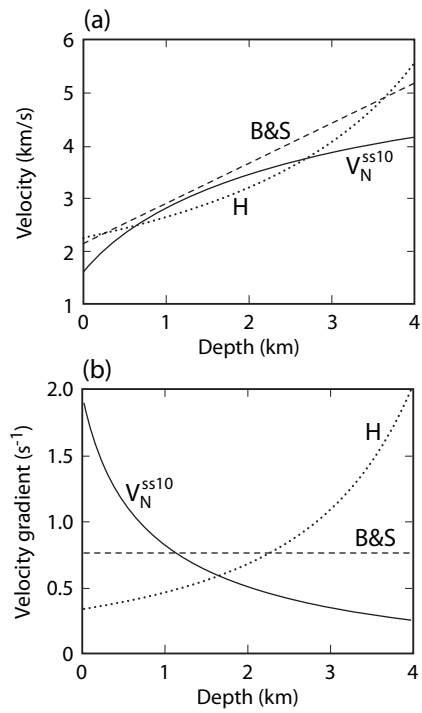
Japsen, Mukerji and Mavko, Fig.08 (1 column)

## Baselines for sandstone and shale



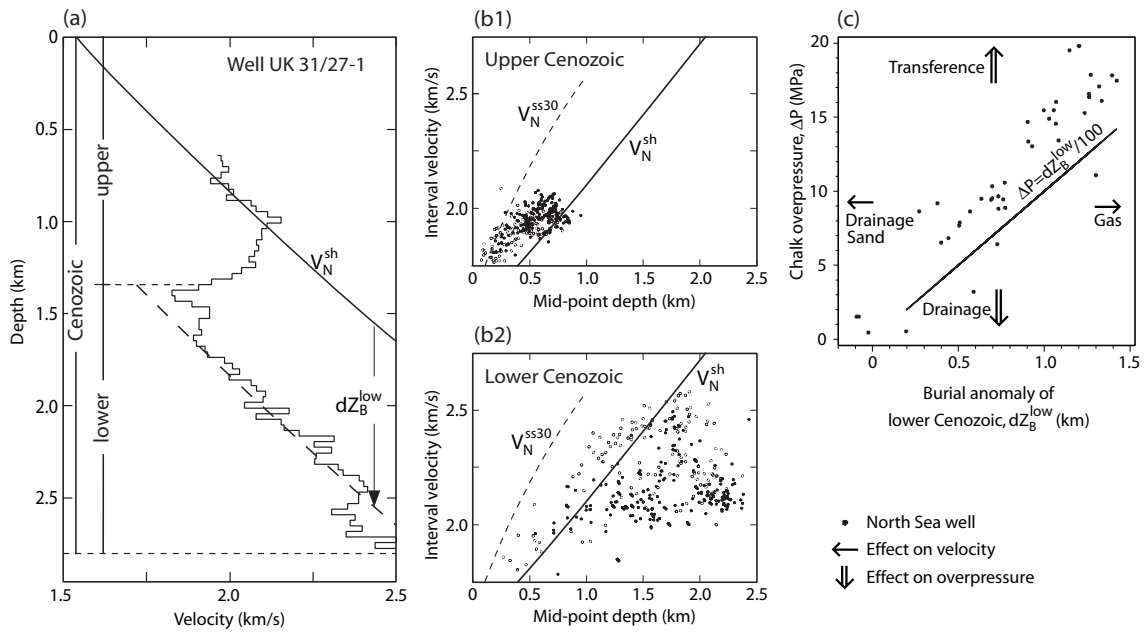
Japsen, Mukerji and Mavko, Fig.09 (1 column)

### Suggested baselines for Bunter Sandstone



Japsen, Mukerji and Mavko, Fig.10 (1 column)

Overpressure-prediction from shale velocity, North Sea



Japsen, Mukerji and Mavko, Fig.11 (2 columns)